Electronic Supplementary Material (ESI) for ChemComm.

Supporting Information

Water activates fresh NiMo foam realizing enhanced urea electrolysis

Experimental section

Materials

Ni foam (labeled as NF, porosity: 96-98%, thickness: 1 mm) and NiMo foam (labeled as NMF, porosity: 96-98%, thickness: 1 mm, atomic ratio of Ni/Mo = 17:3) [1]was purchased from Suzhou Longshengbao Co., Ltd. Potassium hydroxide (KOH) was purchased from Shanghai Meryer Chemical Technology Co. Urea ($CO(NH_2)_2$) were purchased from Sigma-Aldrich Ltd. Hydrochloric acid, ethanol, and acetone were purchased from Beijing Chemical Works. Milli-Q deionized water (resistance of 18.2 MΩ cm at 25 °C) was used for all experiments.

Synthesis of AFNMF (or AFNMF-1h)

In a typical experiment, NMF (10×40 mm, 1 mm in thickness) were ultrasound in acetone and ethanol for 10 min, respectively. The cleaned metal substances were soaked in 3M HCl for 90 min to obtain fresh NiMo foam (labeled as FNMF). Then, FNMF is immersed in deionized water for 60min. After that, the treated NMF was rinsed with ethanol thoroughly. Subsequently, dried in a vacuum oven for 4 h at 60°C. Finally, the sample was named as AFNMF.

Synthesis of AFNMF-1min, AFNMF-10min, AFNMF-1h, AFNMF-3h, AFNMF-6h

Similarly, AFNMF-1min, AFNMF-10min, AFNMF-1h, AFNMF-3h, AFNMF-6h were prepared via a same acid etching and water soaking route, except the time of soaking in deionized water is different (1, 10, 180 and 360 represent different deionized water soaking time (unit: min)). After that, the treated NMF was rinsed

with ethanol thoroughly. The obtained samples are named as AFNMF-1min, AFNMF-10min, AFNMF-3h, AFNMF-6h.

Synthesis of AFNF-1h

In order to compare the role of Mo in electrocatalysis, we prepared AFNF1h. In a typical experiment, NF (10×40 mm, 1 mm in thickness) were ultrasound in acetone and ethanol for 10 min, respectively. The cleaned metal substances were soaked in 3M HCl for 90 min to obtain fresh Ni foam (labeled as FNF). Then, FNF is immersed in deionized water for 60min. After that, the treated NF was rinsed with ethanol thoroughly. Subsequently, dried in a vacuum oven for 4 h at 60°C.

Characterizations

The phase compositions of the catalysts were characterized by X-ray diffraction (XRD, Rigaku SmartLab, operated at 40 kV and 44 mA, parallel beam mode, λ=1.54 Å, step size 0.01 degree and scan rate 1 degree/min). Morphology observation and energy dispersive X-ray (EDX) spectrum analysis were conducted using a Zeiss Ultra 55 field emission scanning electron microscope (SEM). Transmission electron microscopy (TEM) characterization and selected area electron diffraction (SAED) pattern were obtained using an FEI Tecnai G2 20 microscope at 200 kV. X-ray photoelectron spectroscopy (XPS) analysis was performed on an ESCALab MKII spectrometer with Mg Ka X-ray as the excitation source.

Electrochemical Measurement

The electrochemical measurements were carried out in a three-electrode system through the electrochemical workstation (CHI 760E). Hg/HgO was used as the

reference electrode and Pt mesh (1×1 cm) as the counter electrode. HER performances were measured through performing linear sweep voltammetry (LSV, scan rate of 5 mV s^{-1}) in KOH (1.0 M) solution. All of the measured potentials (vs. Hg/HgO) were converted to the potentials against the reversible hydrogen electrode (RHE). All the obtained potentials vs Hg/HgO were converted to RHE according to Nernst equation $E_{RHE}=E_{Hg/HgO}+0.0591pH+0.098$. The long-term durability test was performed using chronopotentiometric measurements. EIS data were collected from 100 kHz to 0.01 Hz at overpotentials of 250 mV with an AC amplitude of 5 mV. All potentials presented were corrected against ohmic potential drop with 95% *iR* compensation. The ECSA was characterized according to a reported method. Specifically, CV (50, 60, 70, 80, and 100 mV s^{-1}) were collected in a narrow potential window of 0.724 V to 0.824 V (vs. RHE) where no faradaic reactions occurred. By plotting the difference of current density (J) between the anodic and cathodic sweeps ($J_{anodic} - J_{cathodic}$) at 0.774 V vs. RHE against the scan rate, a linear trend was observed. The slope of the fitting line is equal to twice the geometric double layer capacitance (C_{dl}), which is proportional to the effective electrode surface area of the materials.

Similarly, the urea electrooxidation reaction (UOR) electrochemical measurements were also carried out in a three-electrode system through the electrochemical workstation (CHI 760E). Hg/HgO was used as the reference electrode and Pt mesh (1×1 cm) as the counter electrode. UOR performances were measured through performing linear sweep voltammetry (LSV, scan rate of 5 mV s^{-1}) in KOH (1.0 M) containing urea with the concentration of 0.5 M. All of the measured potentials (vs.

Hg/HgO) were converted to the potentials against the reversible hydrogen electrode (RHE).

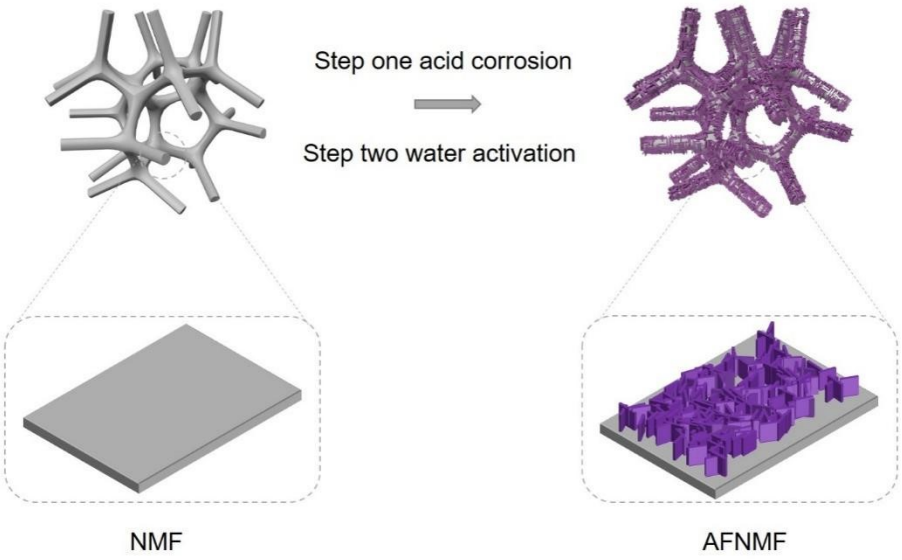

Fig. S1 Synthesis of the AFNMF.

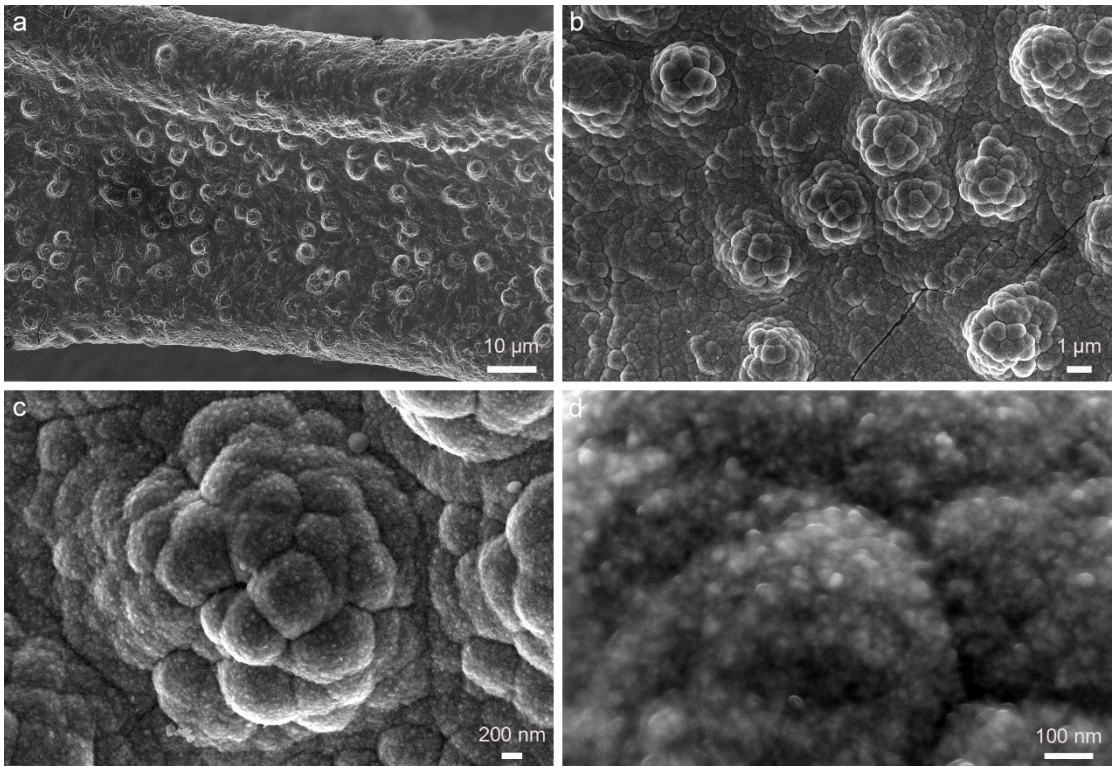

Fig. S2 SEM images of the NMF.

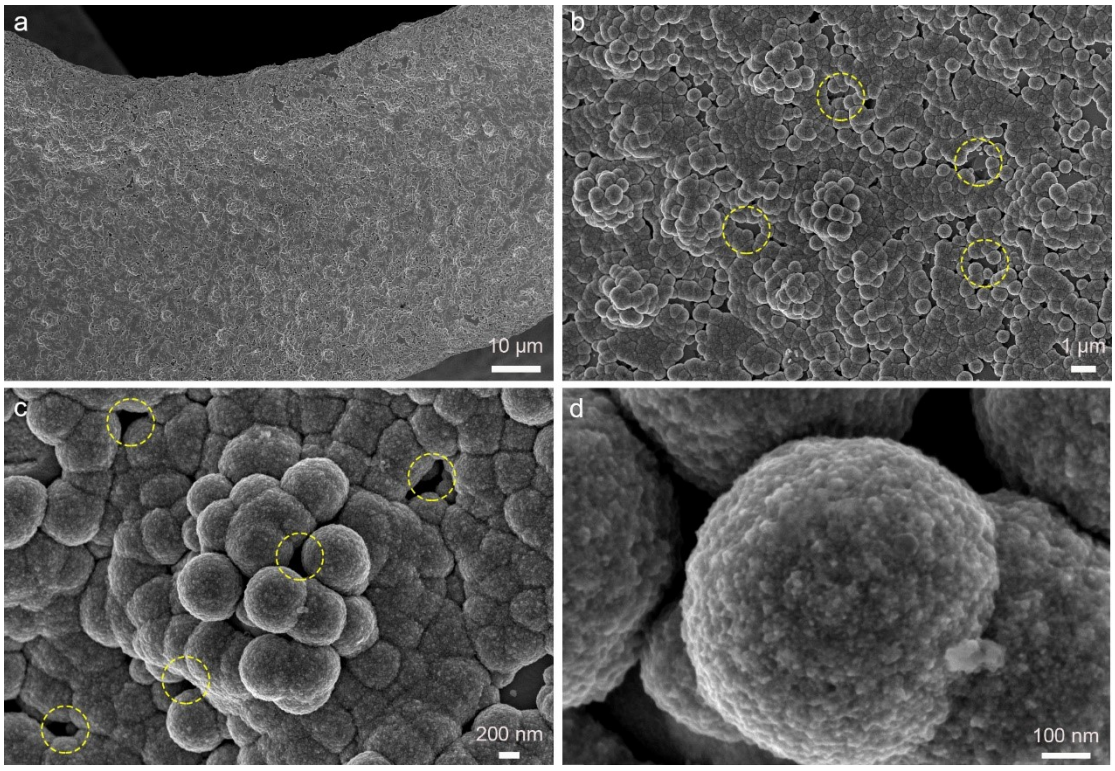

Fig. S3 SEM images of the FNMF (the areas marked with the dotted lines are the etched ravines produced on the surface of the material).

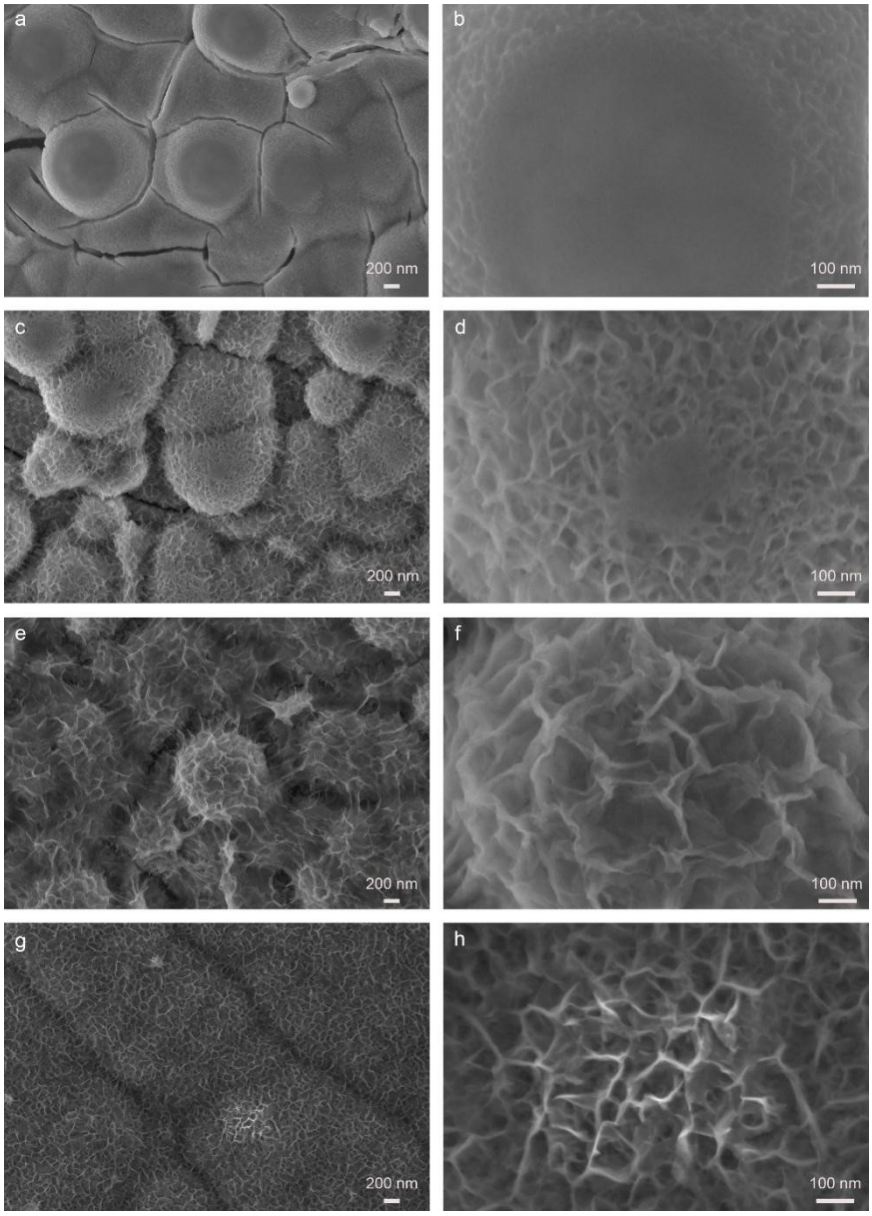

Fig. S4 The SEM images of (a and b) AFNMF1min, (c and d) AFNMF10min, (e and f) AFNMF3h, and (g and h) AFNMF6h.

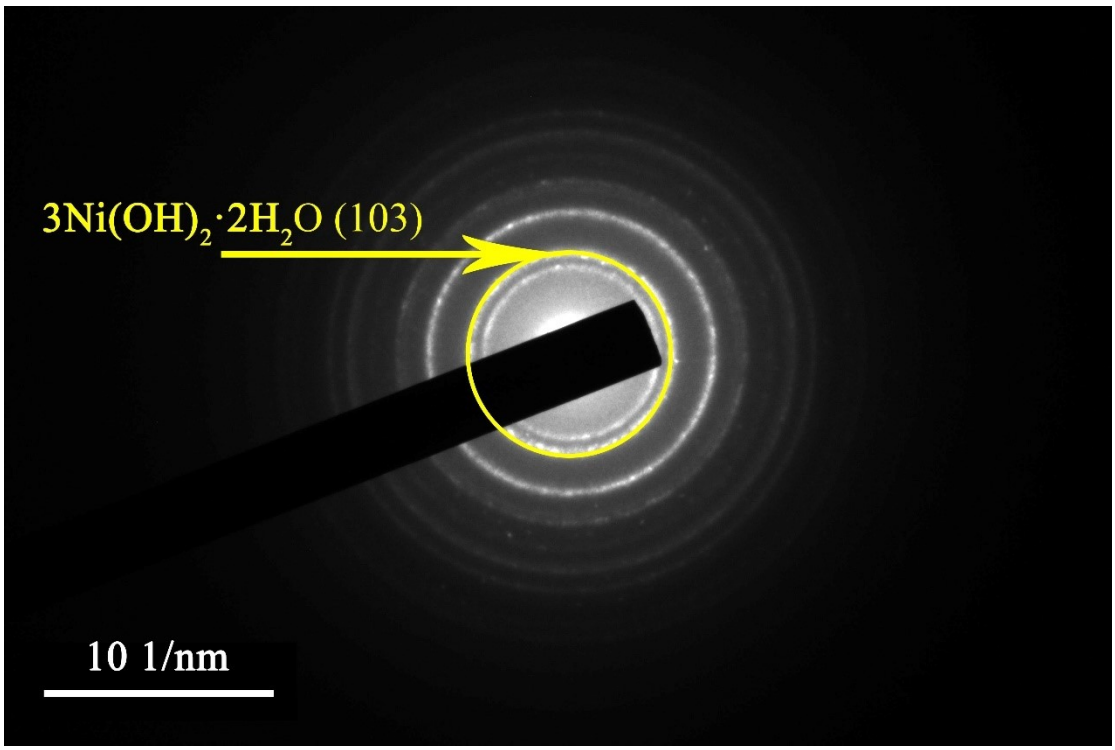

Fig. S5 The SAED image of the AFNMF1h.

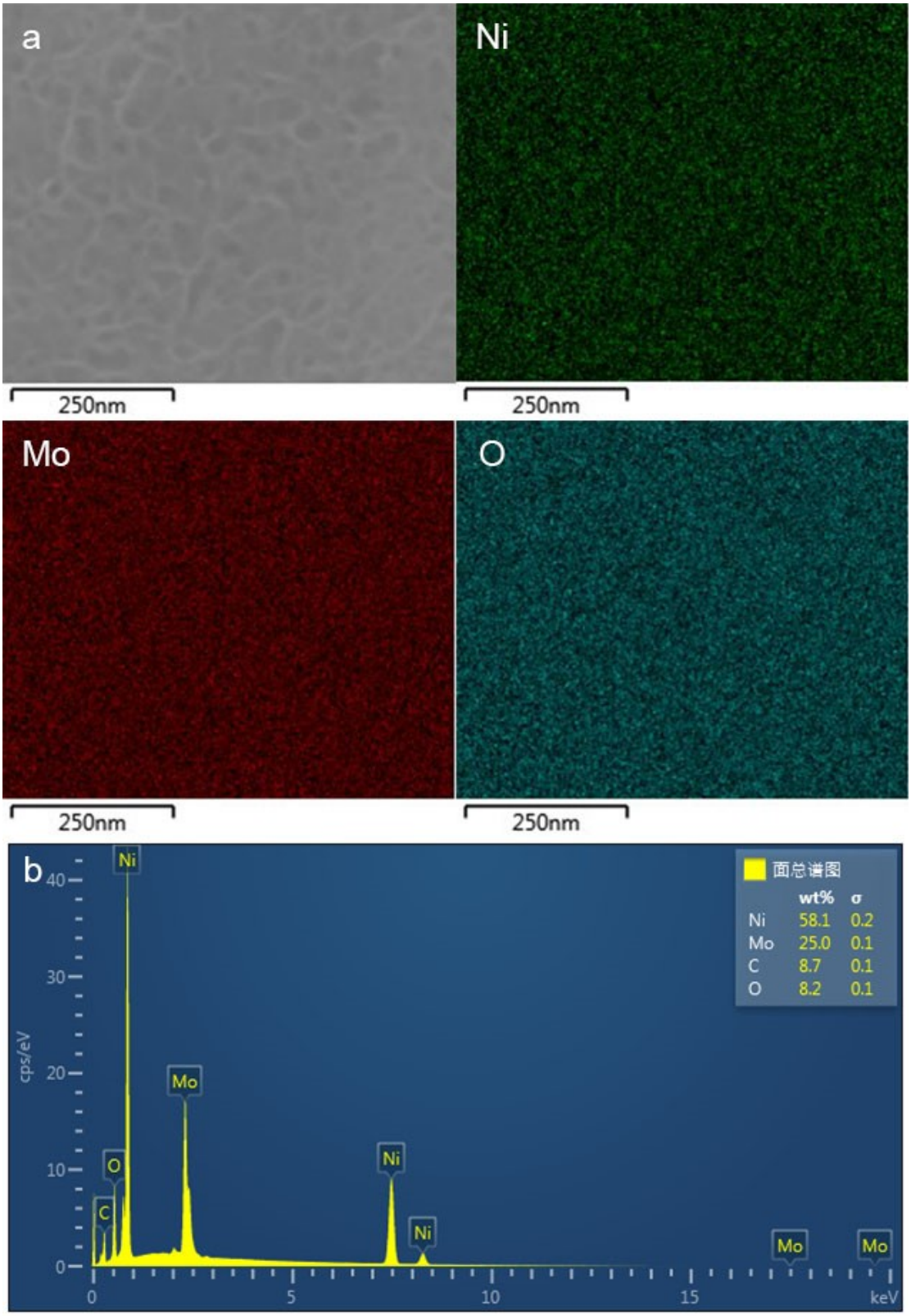

Fig. S6 (a) EDS element mapping images of Ni, Mo and O for the AFNMF1h and (b) element mass distribution of the AFNMF1h.

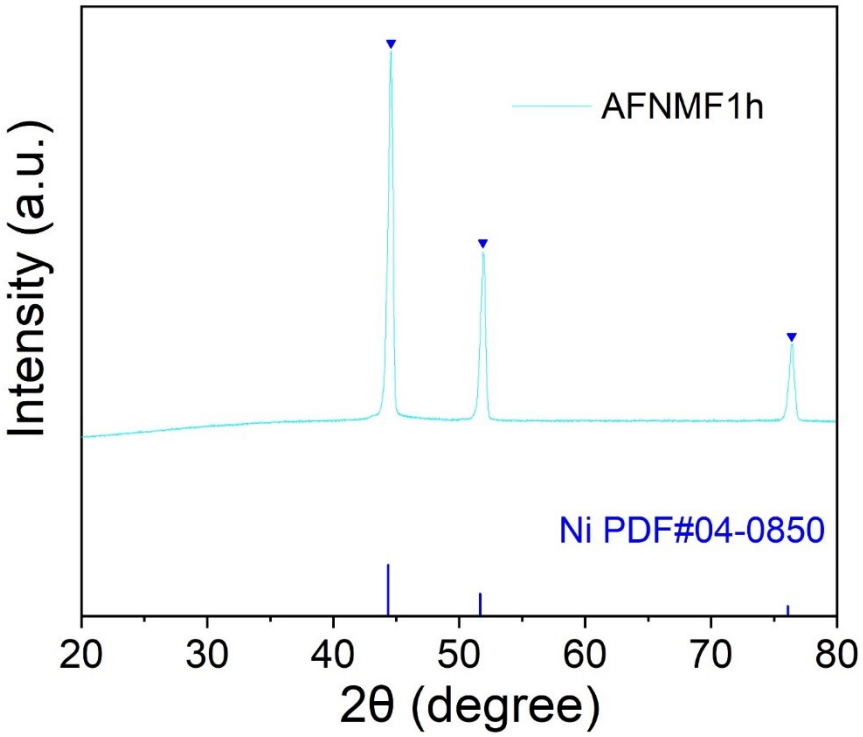

Fig. S7 XRD pattern of AFNMF1h.

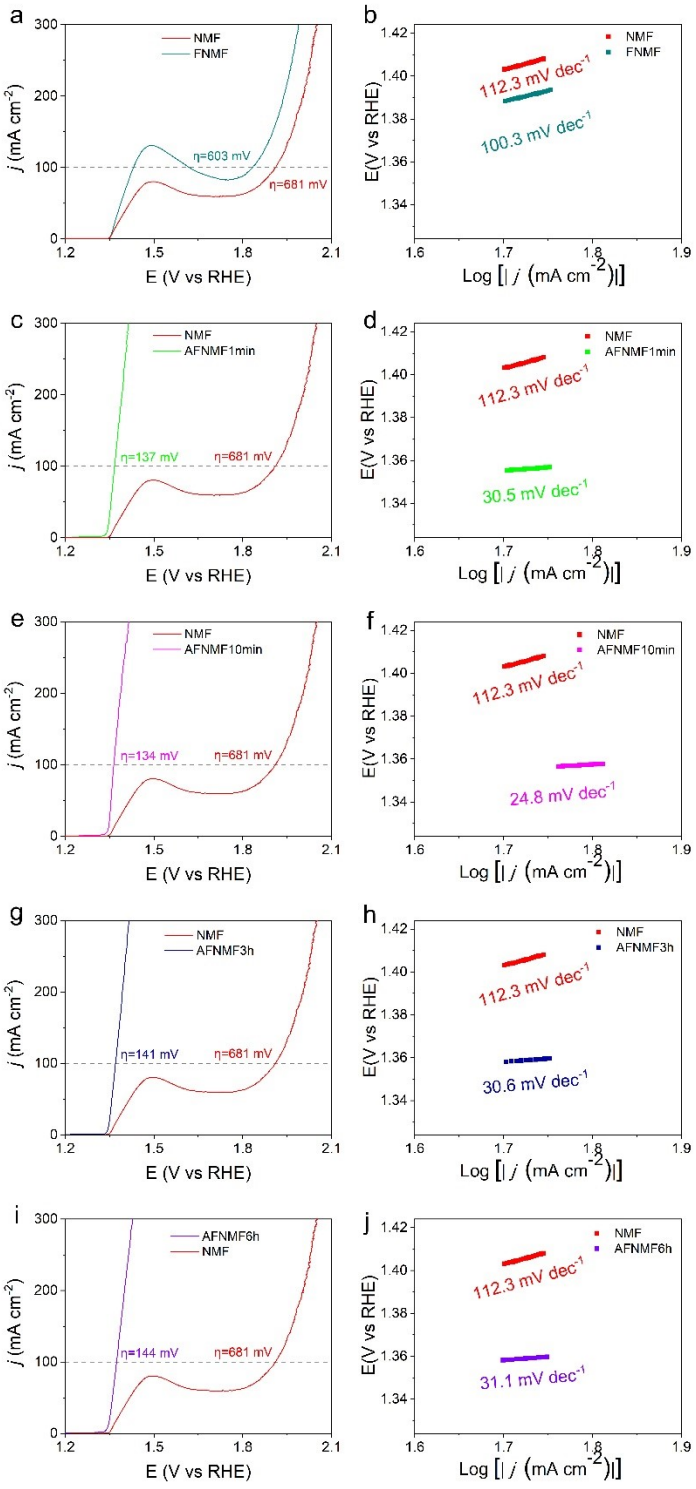

Fig. S8 Electrocatalytic UOR performances. LSV curves and corresponding Tafel plots of (a, b) FNMF, (c, d) AFNMF1min, (e, f) AFNMF10min, (g, h) AFNMF3h and (i, j) AFNMF6h.

The UOR electrochemical performance of the other prepared samples are given in Fig. S8, where the overpotential values of FNMF, AFNMF1min, AFNMF10min, AFNMF3h and AFNMF6h are 603, 137, 134, 141 and 144 mV at 100 mA cm^{-2}, and their Tafel slopes are 100.3, 30.5, 24.8, 30.6, and 31.1 mV dec^{-1}.

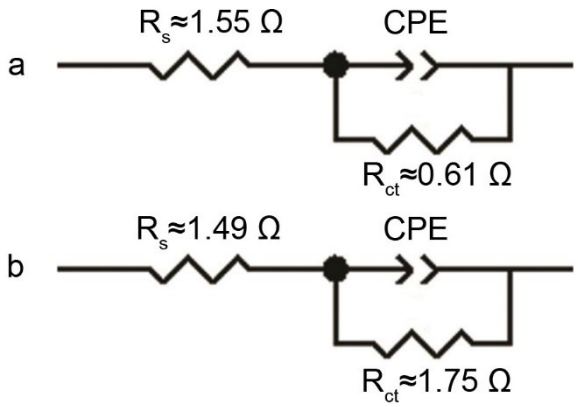

Fig. S9 Equivalent circuit diagram used for fitting impedance spectrum and the corresponding fitting results for UOR: (a) AFNMF1h, (b) NMF. (R_s: equivalent series resistance, R_{ct}: charge transfer resistance, CPE: constant phase angle element.)

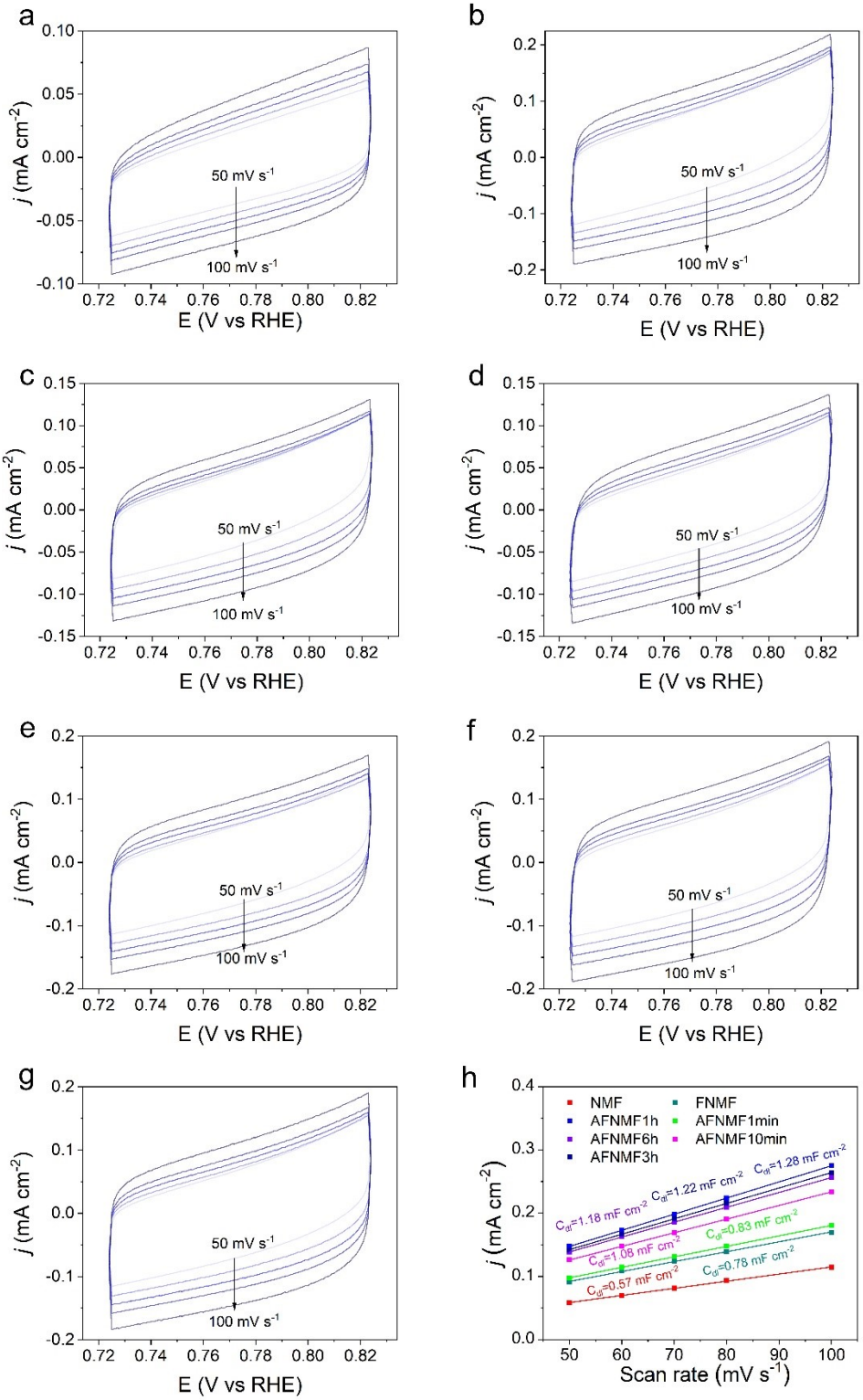

Fig. S10 Cyclic voltammograms curves of (a) NMF (b) AFNMF1h (c) FNMF (d) AFNMF1min (e) AFNMF10min (f) AFNMF3h (g) AFNMF6h (h) C_{dl} plots.

The CV curves of the other prepared samples are given in Fig. S10, where the C_{dl} of FNMF, AFNMF1min, AFNMF10min, AFNMF3h and AFNMF6h are 0.78, 0.83, 1.08, 1.22, and 1.18 mF cm^{-2}.

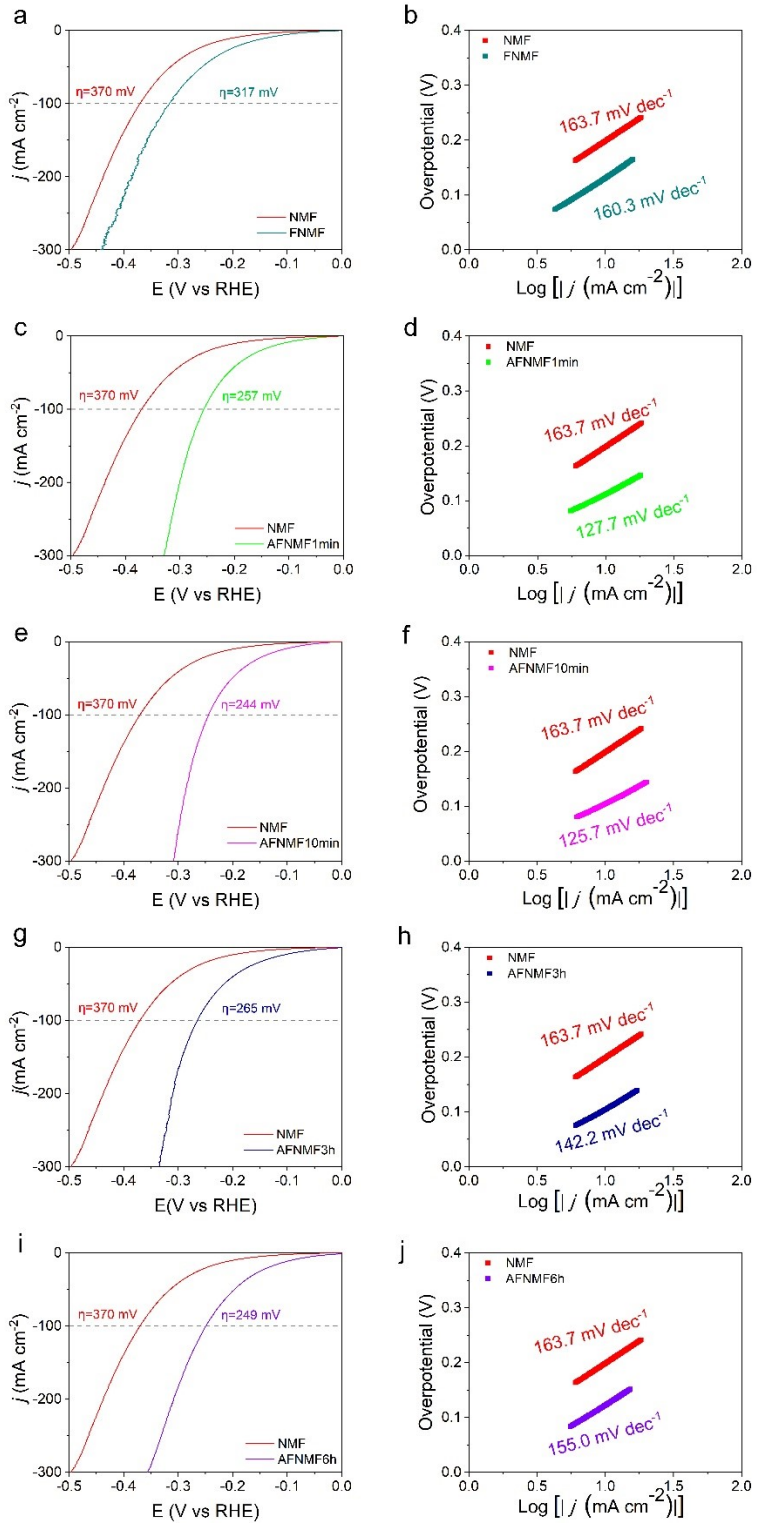

Fig. S11 Electrocatalytic HER performances. LSV curves and corresponding Tafel plots of (a, b) FNMF, (c, d) AFNMF1min, (e, f) AFNMF10min, (g, h) AFNMF3h and (i, j) AFNMF6h.

The HER electrochemical performance of the other prepared samples are given in Fig. S11, where the overpotential values of FNMF, AFNMF1min, AFNMF10min, AFNMF3h and AFNMF6h are 317, 257, 244, 265 and 249 mV at 100 mA cm^{-2}, and their Tafel slopes are 160.3, 127.7, 125.7, 142.2, and 155.0 mV dec^{-1}.

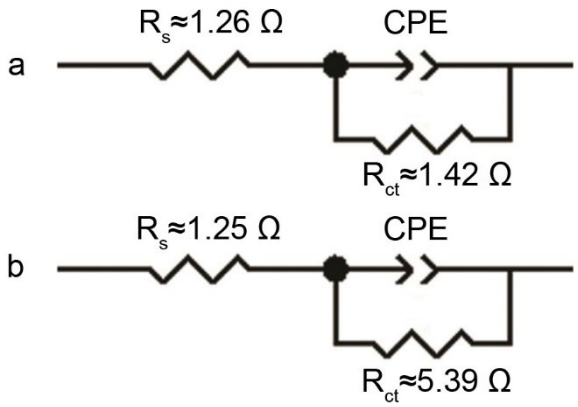

Fig. S12 Equivalent circuit diagram used for fitting impedance spectrum and the corresponding fitting results for HER: (a) AFNMF1h, (b) NMF. (R_s: equivalent series resistance, R_{ct}: charge transfer resistance, CPE: constant phase angle element.)

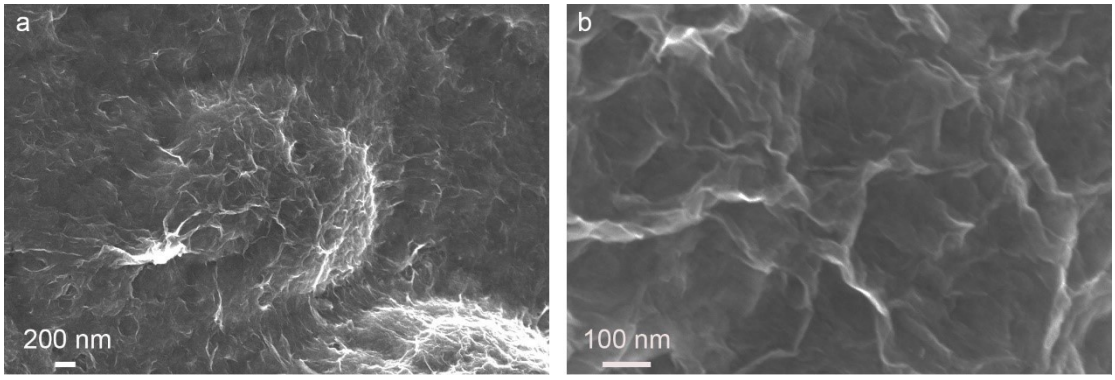

Fig. S13 Typical SEM images of the AFNMF1h after the HER stability test.

Significantly, The SEM images of the AFNMF1h after the chronopotentiometry measurement reveals that the surface of the material still maintains a uniform nanosheet structure and there is no collapse of the structure (Fig.S13).

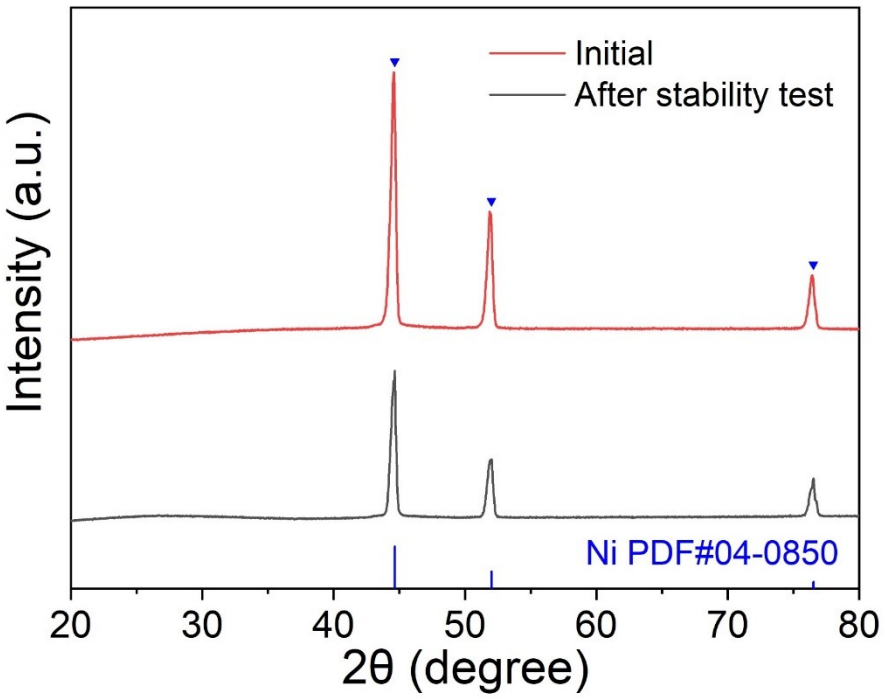

Fig. S14 XRD pattern of AFNMF1h and AFNMF1h after the HER stability test.

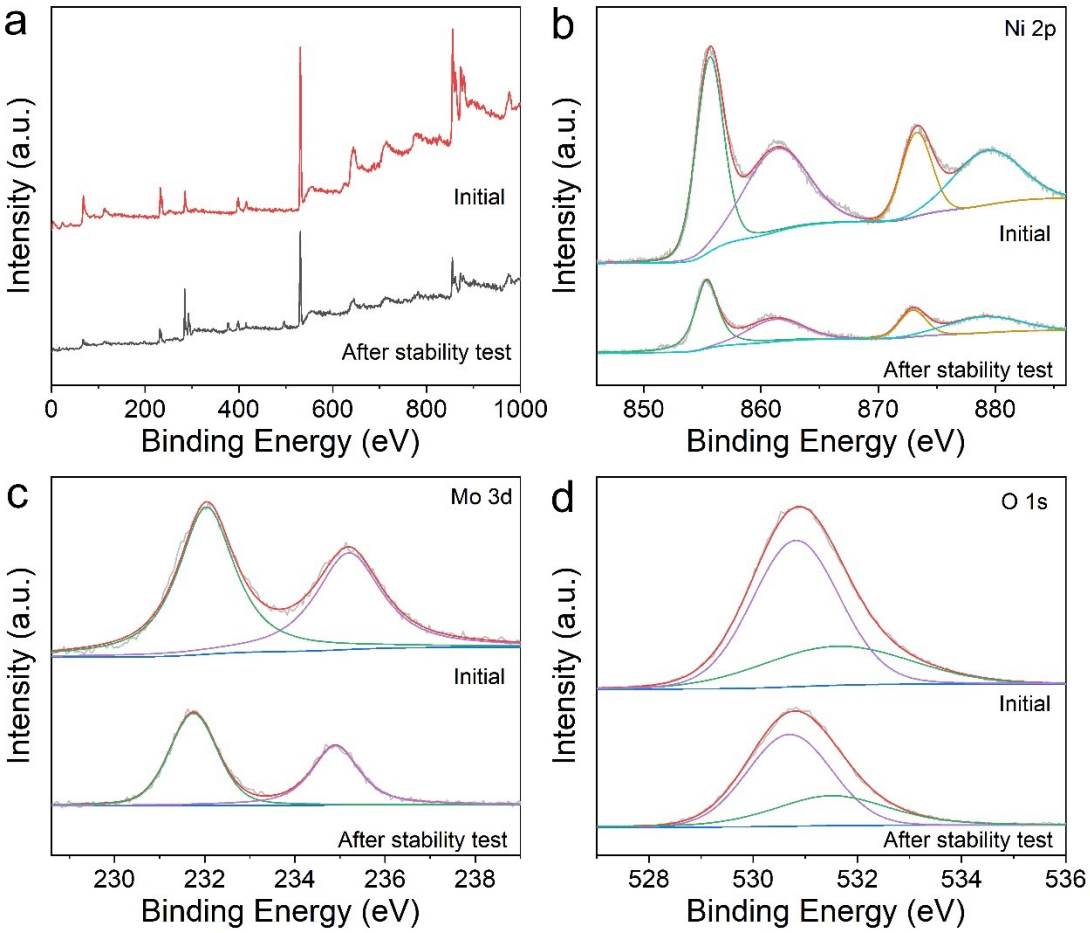

Fig. S15 XPS data of AFNMF1h before and after the HER stability test.

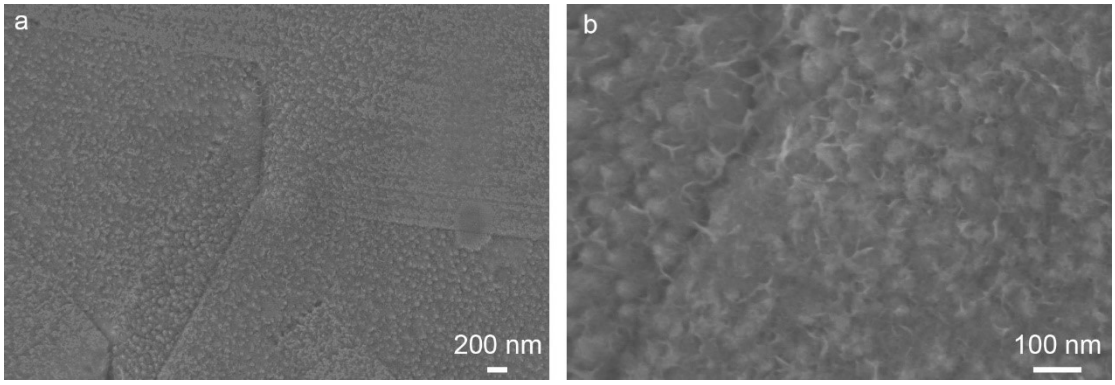

Fig. S16 The SEM images of (a and b) AFNF1h.

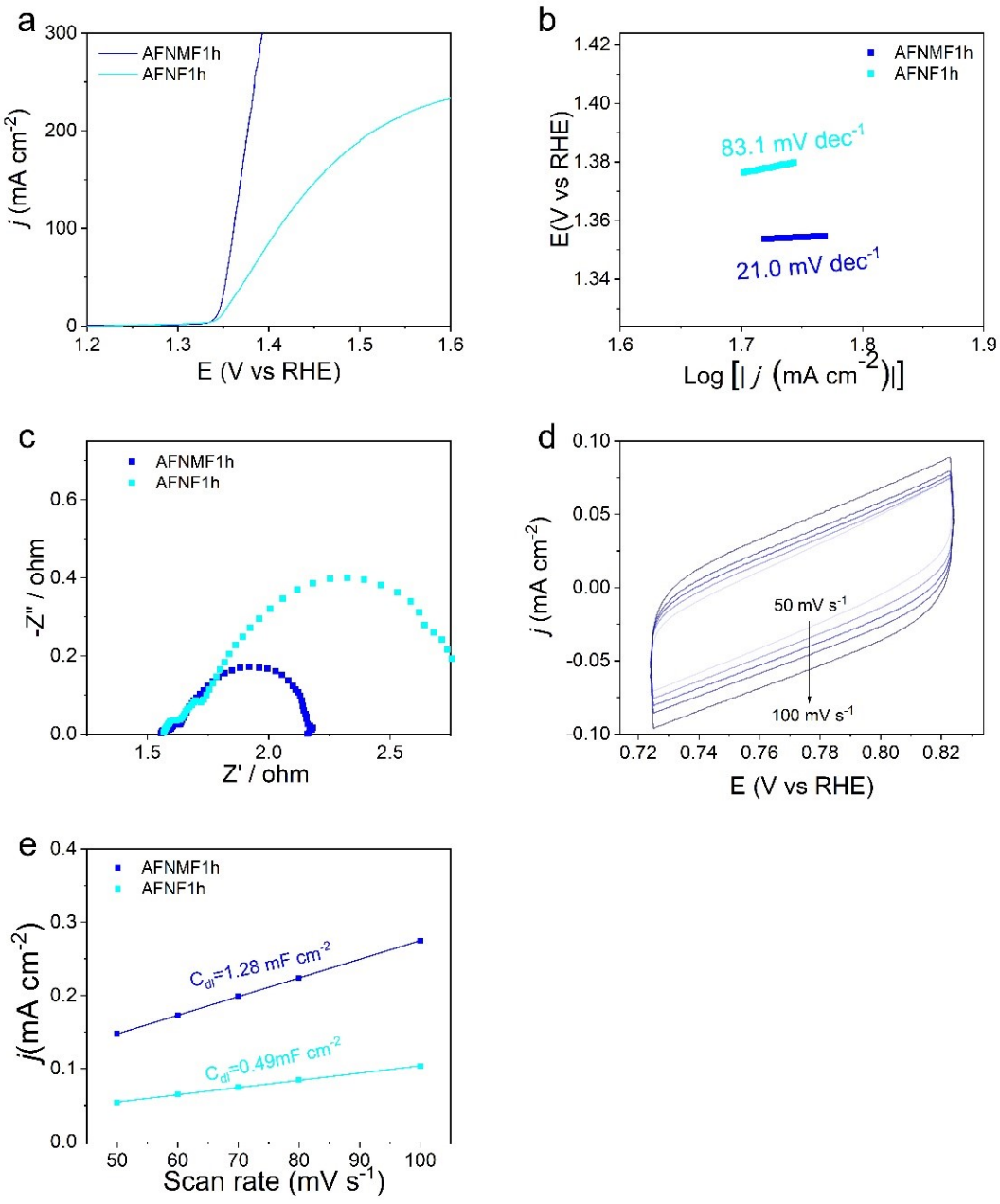

Fig. S17 Electrocatalytic UOR performances. (a) Polarization curves of UOR of AFNMF1h and AFNF1h (b) Tafel plots of the catalysts in UOR. (c) Nyquist plots. (d) Cyclic voltammograms curves of AFNF1h. (e) The C_{dl} plots.

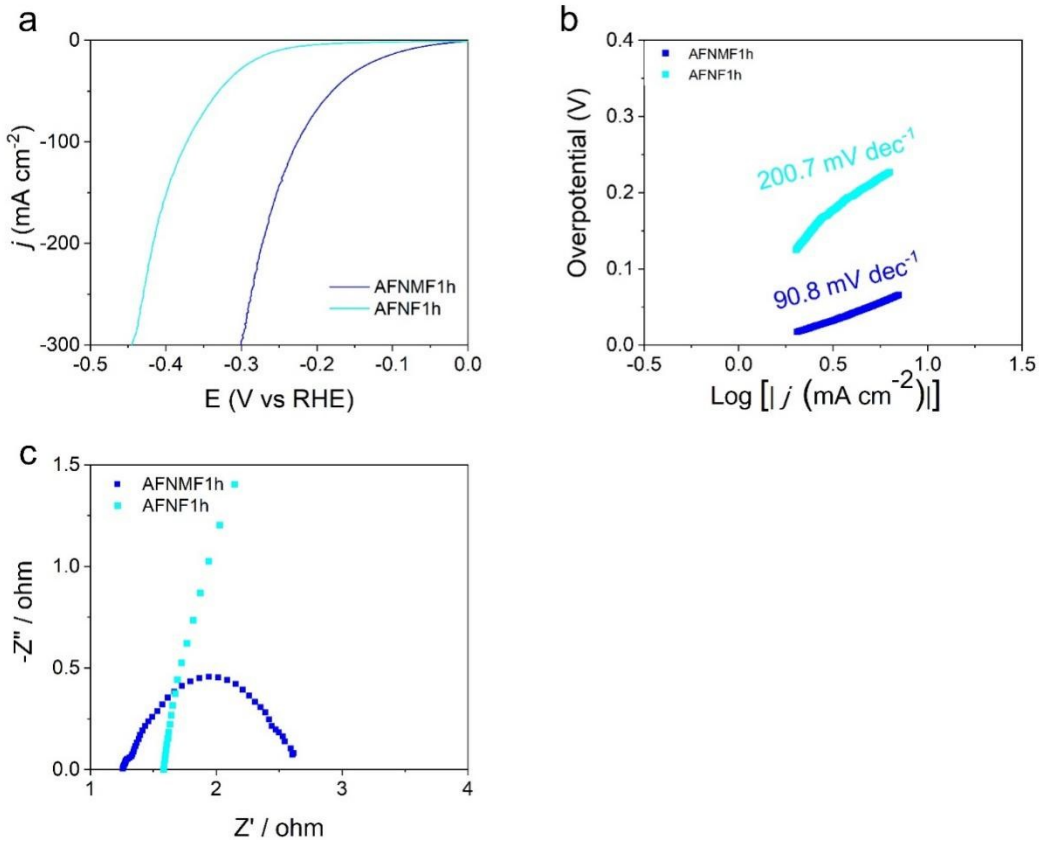

Fig. S18 Electrocatalytic HER performances. (a) Polarization curves of HER of AFNMF1h and AFNF1h (b) Tafel plots of the catalysts in HER. (c) Nyquist plots.

Supplementary Tables

Tab. S1 Comparison of the UOR activity of AFNMF1h with representative Ni-based catalysts.

catalysts	Electrolyte	Potential (V vs. RHE) @*j*=100 mA cm^{-2}	Reference
AFNMF-1h	1 M KOH and 0.5 M urea	1.36	This work
S-NiFeV LDH	1 M KOH and 0.33 M urea	1.38	2
NiFe NCs/GO	1 M KOH and 0.5 M urea	1.45	3
2D-MnO_2-550	1 M KOH and 0.33 M urea	1.42	4
C–NP– NCOH	1 M KOH and 0.5 M urea	1.38	5
NiMoCu-NF	1 M KOH and 0.33 M urea	1.40	6
$Cr_{0.4}$-Co_2P/NF	1 M KOH and 0.5 M urea	1.362	7
RuFe/Ni_5P_4	1 M KOH and 0.33 M urea	1.38	8
NCMO–Ar	1 M KOH and 0.5 M urea	1.38	9
CoNiFeS–OH	1 M KOH and 0.33 M urea	1.373	10
Co-Mn-Fe_9S_{11}@Ni_9S_8/NF	1 M KOH and 0.5 M urea	1.41	11

References

1 X. Liu, Y. Yang, X. Xing, T. Zou, Z. Wang and Y. Wang, *ChemElectroChem*, 2017, **5**, 434-444.

2 K. Peng, L. Liu, N. Bhuvanendran, F. Qiao, G. Lei, S. Y. Lee, Q. Xu and H. Su, *Materials Advances*, 2023, 1354-1362.

3 X. Ge, L. Yin, L. Zhang, C. Shi, Q. Shen, W. Ma, X. Yang, Y. Sun and C. Li, *CrystEngComm*, 2023, **25**, 925-934.

4 Y. Shi, J. Li, X. Zhang, K. Zhao, Z. Wang, Z. Wang and X. Peng, *RSC Adv*, 2022, **12**, 30605-30610.

5 Y. Wang, C. Zhang, X. Du and X. Zhang, *Dalton Trans*, 2022, **51**, 14937-14944.

6 R. Li, Y. Yuan, H. Gui, Y. Liu, H. Li, Y. Li, S. Wen, A. Liu, J. Zhang, P. Yang and M. An, *Nanoscale*, 2022, **14**, 14297-14304.

7 X. Li, X. Du and X. Zhang, *Dalton Trans*, 2022, **51**, 13255-13262.

8 W. Xu, W. Zhang, Z. Sun, L. Guo, L. Xie, C. Li, Y. Feng, Q. Liang, Y. Yang and H.-b. Sun, *Sustainable Energy & Fuels*, 2022, **6**, 4153-4159.

9 X. Liu, H. Qin, G. Wang, Q. Li, Q. Huang, Z. Wen and S. Mao, *Journal of Materials Chemistry A*, 2022, **10**, 16825-16833.

10 C. Fang, D. Zhang, X. Wang and R. Li, *Inorganic Chemistry Frontiers*, 2022, **9**, 3643-3653.

11 J. Li, L. Zhang, X. Du and X. Zhang, *Dalton Trans*, 2022, **51**, 10249-10256.